
Superior Energy Storage Performance in High-Entropy Dielectric Ceramics Discovered by AI Materials Scientist

Anonymous Author(s)

Affiliation

Address

email

Abstract

The design of advanced energy storage materials is hindered by vast and complex compositional spaces that are intractable for traditional trial-and-error methodologies. High-entropy ceramics (HECs) represent a promising class of dielectrics, but their multi-element nature exponentially expands this search space. To address this challenge, we deployed an ‘AI Materials Scientist’—an autonomous research agent—to navigate the high-dimensional landscape of lead-free perovskite HECs. The AI agent successfully identified a novel, non-intuitive five-component composition: $0.36\text{BaTiO}_3\text{--}0.32\text{BiFeO}_3\text{--}0.09\text{Bi}_{0.5}\text{Na}_{0.5}\text{TiO}_3\text{--}0.19\text{CaZrO}_3\text{--}0.04\text{Sr}_{0.7}\text{La}_{0.2}\text{TiO}_3$. Experimental synthesis and characterization validated the AI’s prediction, revealing a phase-pure ceramic with a dense, fine-grained microstructure. This material exhibits a breakthrough recoverable energy density (W_{rec}) of 10 J/cm^3 and a high energy efficiency (η) of 80% at a breakdown strength of $\sim 850 \text{ kV/cm}$, outperforming most existing lead-free dielectric ceramics. This work not only introduces a state-of-the-art energy storage material but also demonstrates the transformative potential of AI-driven autonomous systems to accelerate the discovery of complex, high-performance materials.

17

1 Introduction

18 As global reliance on renewable energy and electrification technologies deepens, the development of
19 advanced energy storage devices has become critical for technological progress [1]. In particular,
20 high-performance dielectric capacitors are indispensable components in pulsed power systems that
21 demand high power density and rapid energy release, such as in advanced radar, electric vehicles,
22 and medical equipment [2,3]. Among various candidate materials, dielectric ceramics are considered
23 one of the most promising for next-generation high-power applications due to their high permittivity,
24 excellent thermal resistance, and robust chemical stability [4].

25 To enhance energy storage performance, defined by recoverable energy density (W_{rec}) and efficiency
26 (η), researchers have traditionally focused on the compositional modification of classic perovskite
27 ceramics such as BaTiO_3 and BiFeO_3 [5,6]. However, conventional design strategies often encounter
28 a trade-off dilemma, where the synergistic optimization of dielectric constant and breakdown strength
29 is difficult to achieve [7], thereby limiting breakthroughs in energy density. Recently, the concept of
30 high-entropy ceramics (HECs) has emerged as a novel paradigm to overcome this bottleneck [8]. By
31 incorporating five or more principal cations into a single lattice, the high-entropy effect can induce
32 unique microstructures and pronounced relaxor behavior, offering the potential to discover ‘islands’
33 of superior properties within highly complex compositional landscapes [9,10].

34 While the high-entropy strategy is promising, it presents an unprecedented challenge: a dimensionally
35 explosive and virtually infinite chemical space [11]. Within this high-dimensional space,

36 the relationship between composition and material properties is highly non-linear, rendering the
37 traditional Edisonian ‘trial-and-error’ approach—which relies heavily on researchers’ experience and
38 intuition—ineffective [12]. Exploring this vast landscape manually is akin to searching for a needle in
39 a haystack. Consequently, the development of a new paradigm capable of intelligently navigating this
40 complex compositional space to accelerate the discovery of high-performance materials has become
41 imperative [13].

42 To address this challenge, we moved beyond conventional R&D models and entrusted the task
43 of materials discovery to an ‘AI Materials Scientist’. This AI agent, powered by deep learning
44 on a vast body of published material data, establishes complex composition-structure-property
45 relationships and is empowered to autonomously explore and create novel formulations [14,15].
46 In this work, we deployed the AI Materials Scientist to navigate the uncharted territory of high-
47 entropy ceramics. It successfully proposed and identified a novel five-component, lead-free high-
48 entropy ceramic: $0.36\text{BaTiO}_3 - 0.32\text{BiFeO}_3 - 0.09\text{Bi}_{0.5}\text{Na}_{0.5}\text{TiO}_3 - 0.19\text{CaZrO}_3 - 0.04\text{Sr}_{0.7}\text{La}_{0.2}\text{TiO}_3$.
49 Subsequent experimental synthesis and characterization confirmed the breakthrough nature of this
50 discovery: the ceramic exhibits a superior recoverable energy storage density of 10 J/cm^3 and a high
51 efficiency of 80%, outperforming most previously reported lead-free dielectric ceramics [16,17]. This
52 paper details the AI’s design process alongside the structural, microstructural, and exceptional energy
53 storage properties of the novel ceramic, thereby validating the immense potential of AI as a research
54 partner in accelerating scientific discovery [18].

55 2 Methods

56 2.1 System architecture of the AI Materials Scientist

57 The AI agent constructed in this work, the AI Materials Scientist, operates within a human-machine
58 collaboration framework. The high-level design of this system is intended to comprehensively enhance
59 and accelerate the end-to-end materials research workflow—from initial knowledge acquisition
60 to final experimental validation. Its system architecture is composed of three core engines: the
61 Knowledge Engine, the Exploration Engine, and the Experiment Engine. These engines operate both
62 independently and collaboratively.

63 **Knowledge Engine** The Knowledge Engine serves as the cognitive core of the AI Materials
64 Scientist, with its primary mission being the construction of a comprehensive, multi-modal knowledge
65 base that surpasses human capabilities. It integrates heterogeneous data from diverse sources,
66 including scientific literature, specialized databases, and knowledge graphs. The engine leverages
67 Large Language Models (LLMs) and prompt engineering techniques to achieve automated extraction
68 and structured processing of key information—such as material compositions, processing protocols,
69 and performance metrics—from unstructured text. Through deep learning models optimized for
70 materials science, the engine further integrates this textual information with physicochemical features
71 to support complex knowledge mining and property prediction tasks.

72 **Exploration Engine** The Exploration Engine functions as the innovation and decision-making
73 core of the AI Materials Scientist, specifically designed for the efficient exploration of the high-
74 dimensional and complex compositional spaces inherent in materials research. This engine integrates
75 a suite of advanced machine learning algorithms, including active learning, Bayesian optimization,
76 and generative adversarial networks, enabling it to accurately predict the potential performance
77 of new materials based on existing knowledge. Its core capability lies in intelligent experimental
78 design, where it identifies the most valuable candidate formulations by optimizing experimental plans,
79 thereby replacing the traditional trial-and-error paradigm and accelerating the discovery of materials
80 with breakthrough performance using a minimal number of iterations.

81 **Experiment Engine** The Experiment Engine is the physical execution terminal of the AI Materials
82 Scientist, responsible for transforming the digital design blueprints generated by the preceding
83 engines into tangible physical samples and experimental data. This engine integrates and controls
84 an end-to-end automated robotic hardware platform, with capabilities covering the entire materials
85 preparation and characterization process, from high-precision powder dispensing, ball milling, and
86 pellet pressing to automated electrical property measurements. This achieves a high degree of

87 automation in experimental operations, with only a few non-standard or complex steps requiring
88 manual assistance.

89 The synergistic integration of the three engines described above establishes a complete “design-
90 manufacture-test-learn” closed-loop autonomous research system (Self-driving Laboratory). In this
91 workflow, the Exploration Engine first proposes a new material formulation design. The Experiment
92 Engine then automatically completes the sample preparation and performance characterization,
93 feeding the newly acquired experimental data back to the Knowledge Engine for absorption and
94 integration. Once the knowledge base is updated, the Exploration Engine can proceed with the next,
95 more optimized design iteration.

96 **2.2 Ceramic preparation**

97 The high-entropy dielectric ceramic with the composition $0.36\text{BaTiO}_3\text{--}0.32\text{BiFeO}_3\text{--}0.09\text{Bi}_{0.5}\text{Na}_{0.5}\text{TiO}_3\text{--}0.19\text{CaZrO}_3\text{--}0.04\text{Sr}_{0.7}\text{La}_{0.2}\text{TiO}_3$ was fabricated using a conventional
98 solid-state reaction method. High-purity raw materials, including BaCO_3 (Aladdin, 99.8%), Bi_2O_3
99 (Aladdin, 99.9%), Fe_2O_3 (Aladdin, 99.9%), TiO_2 (Aladdin, 99.8%), Na_2CO_3 (Aladdin, 99.9%),
100 CaCO_3 (Aladdin, 99.5%), ZrO_2 (Aladdin, 99.9%), SrCO_3 (Aladdin, 99.9%), and La_2O_3 (Aladdin,
101 99.9%) were used as starting powders.

102 The powders were weighed according to the stoichiometric ratio, with an additional 5 wt% excess of
103 Bi_2O_3 added to compensate for potential bismuth volatilization during high-temperature sintering.
104 The weighed powders were placed in a nylon jar with zirconia balls and ball-milled in ethanol for
105 24 hours to ensure homogeneous mixing. After milling, the slurry was dried at 100°C for 12 hours
106 and then calcined at 850°C for 4 hours in a muffle furnace.

107 The calcined powders were subsequently ball-milled again for 24 hours to reduce agglomeration.
108 The resulting fine powder was dried, mixed with a polyvinyl alcohol (PVA) solution as a binder, and
109 pressed into pellets 10 mm in diameter under a pressure of 200 MPa. The green pellets were heated
110 to 600°C for 4 hours to burn out the binder, followed by sintering in a range of 1150–1250°C for
111 4 hours in air. The sintered pellets were then polished to a final thickness of 50–100 μm , and circular
112 gold (Au) electrodes with an area of 0.00785 cm^2 were sputtered onto both surfaces for electrical
113 measurements.

115 **3 Results and discussion**

116 **3.1 Crystal structure analysis**

117 To determine the phase composition and crystal structure of the AI-designed ceramic, X-ray diffraction
118 (XRD) was conducted at room temperature. Figure 1 shows the XRD pattern of the sintered
119 $0.36\text{BaTiO}_3\text{--}0.32\text{BiFeO}_3\text{--}0.09\text{Bi}_{0.5}\text{Na}_{0.5}\text{TiO}_3\text{--}0.19\text{CaZrO}_3\text{--}0.04\text{Sr}_{0.7}\text{La}_{0.2}\text{TiO}_3$ ceramic, scanned
120 over a 2θ range from 20° to 80°. All major diffraction peaks can be unambiguously indexed to
121 a single-phase perovskite structure, consistent with standard perovskite reference patterns (e.g.,
122 PDF#22-0153 for BaTiO_3). No secondary or impurity phases were detected within the instrument’s
123 resolution limit, confirming that the five components have thoroughly diffused into the host lattice to
124 form a chemically homogeneous solid solution.

125 The pattern displays all characteristic reflections of the perovskite lattice. The most intense peak, a
126 hallmark of the perovskite structure, appears at $2\theta \approx 31.4^\circ$ and corresponds to the (110) plane. Other
127 principal peaks observed at approximately 22.5°, 38.7°, 45.0°, 56.0°, and 65.7° are indexed to the
128 (100), (111), (200), (211), and (220) planes, respectively. The sharpness and high intensity of these
129 peaks indicate a high degree of crystallinity, implying that the designed composition and solid-state
130 reaction route promote the development of a well-ordered crystal structure.

131 Closer inspection of the reflections—particularly the (200) peak near 45.0°—shows a symmetric
132 profile without noticeable splitting, suggesting that the multicomponent ceramic adopts a pseudocubic
133 symmetry. The high configurational entropy resulting from the incorporation of multiple cations
134 with diverse ionic sizes and valences at both A-sites (Ba^{2+} , Bi^{3+} , Na^+ , Ca^{2+} , Sr^{2+} , La^{3+}) and
135 B-sites (Ti^{4+} , Fe^{3+} , Zr^{4+}) likely suppresses the formation of long-range polar domains typical
136 of simpler perovskites, thereby stabilizing a highly symmetric lattice. This result is critical, as it
137 experimentally validates the AI’s underlying hypothesis: the novel, complex composition is not only

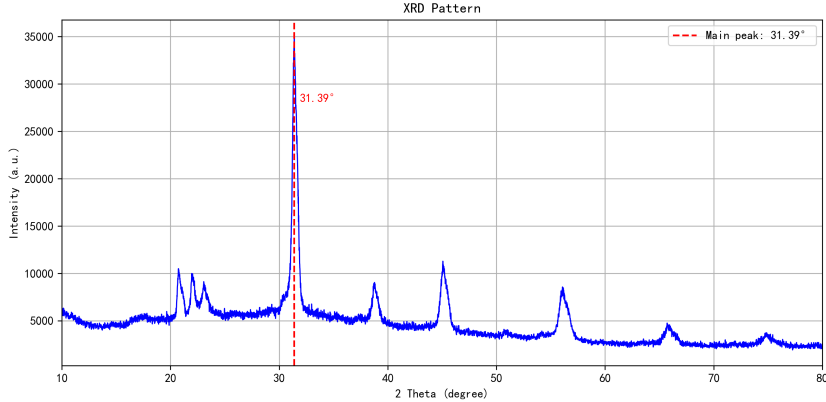


Figure 1: X-ray diffraction pattern of the AI-designed high-entropy ceramic $0.36\text{BaTiO}_3\text{--}0.32\text{BiFeO}_3\text{--}0.09\text{Bi}_{0.5}\text{Na}_{0.5}\text{TiO}_3\text{--}0.19\text{CaZrO}_3\text{--}0.04\text{Sr}_{0.7}\text{La}_{0.2}\text{TiO}_3$ sintered at optimal temperature.

138 synthesizable but also crystallizes into a phase-pure perovskite structure—providing the essential
139 structural foundation for achieving superior energy storage performance.

140 3.2 Microstructural analysis

141 Following the phase identification, the microstructure of the ceramic, which is critically linked to its
142 electrical properties, was investigated using scanning electron microscopy (SEM). Figure 2 displays
143 the micrograph of the as-sintered surface of the AI-designed high-entropy ceramic. The image
144 reveals a highly dense and uniform microstructure, composed of fine, sub-micron sized grains with
145 a generally spherical or slightly irregular morphology. The average grain size is estimated to be
146 in the range of 200–500 nm. The grains are observed to be tightly packed with well-defined grain
147 boundaries, and there is a notable absence of large pores, voids, or microcracks. This indicates that a
148 high relative density was successfully achieved through the solid-state sintering process, which is a
149 crucial prerequisite for high-performance dielectric materials.

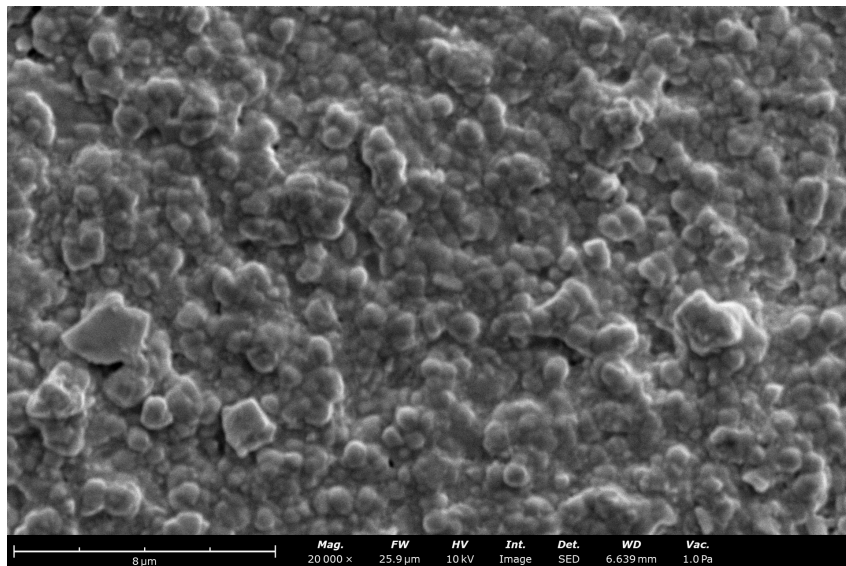


Figure 2: Scanning electron microscopy (SEM) micrograph of the as-sintered surface of the $0.36\text{BaTiO}_3\text{--}0.32\text{BiFeO}_3\text{--}0.09\text{Bi}_{0.5}\text{Na}_{0.5}\text{TiO}_3\text{--}0.19\text{CaZrO}_3\text{--}0.04\text{Sr}_{0.7}\text{La}_{0.2}\text{TiO}_3$ high-entropy ceramic

150 The observed microstructural characteristics are fundamentally important for the superior energy
151 storage performance of this ceramic. Firstly, the high density is essential for ensuring high dielectric
152 breakdown strength (E_b). Pores and voids, which have extremely low breakdown strength, can
153 cause local electric field concentration, leading to premature dielectric breakdown and a catastrophic
154 failure of the device at low applied fields. The dense structure observed here minimizes these defects,
155 allowing the material to withstand a much higher electric field before breaking down. According to
156 the energy storage formula ($W_{\text{rec}} \approx \frac{1}{2}\varepsilon_0\varepsilon_r E_b^2$), this enhancement in E_b is the most effective way to
157 drastically increase the energy storage density.

158 Secondly, the fine-grained nature of the ceramic plays a pivotal twofold role. On one hand, the
159 proliferation of grain boundaries in a fine-grained material acts as an effective barrier to the propa-
160 gation of electrical breakdown channels, further enhancing the overall breakdown strength. On the
161 other hand, the small grain size can disrupt the long-range ferroelectric order, promoting relaxor-like
162 behavior. This leads to the development of slim polarization-electric field (P-E) hysteresis loops
163 with low remnant polarization (P_r), which directly translates to lower energy loss (W_{loss}) and conse-
164 quently, higher energy storage efficiency (η). Therefore, the combination of high densification and a
165 fine-grained microstructure, as observed in Figure 2, provides the ideal microstructural foundation
166 for the simultaneous realization of high breakdown strength and high efficiency, corroborating the
167 outstanding performance metrics achieved by the AI-designed material.

168 3.3 Energy storage performance analysis

169 To evaluate the energy storage capabilities of the AI-designed high-entropy ceramic, the polarization-
170 electric field (P-E) hysteresis loops were measured at room temperature under various applied electric
171 fields. Figure 3 presents the resulting P-E loops, which provide direct insight into the material's
172 dielectric and ferroelectric response. A series of remarkably slim and slanted loops were observed,
173 which is a hallmark characteristic of relaxor ferroelectrics or linear dielectrics, ideal for energy
174 storage applications. Even at the maximum applied electric field of approximately 850 kV/cm, the
175 ceramic exhibits a very low remnant polarization (P_r) and coercivity, indicating that the polarization
176 can return to near zero upon removal of the field. This behavior leads to a large difference between
177 the maximum polarization ($P_{\text{max}} \approx 33 \mu\text{C}/\text{cm}^2$) and the remnant polarization (P_r), which is critical
178 for obtaining high recoverable energy density. The slim nature of the loops signifies minimal energy
179 dissipation during the charge-discharge cycle, predicting a high energy storage efficiency.

180 The quantitative energy storage performance, including the recoverable energy density (W_{rec}) and
181 efficiency (η), was calculated from the P-E loop data and is plotted as a function of the applied
182 electric field in Figure 4. The recoverable energy density (W_{rec} , purple curve) is observed to increase
183 monotonically with the electric field, reaching a remarkable value of 10 J/cm³ at a breakdown strength
184 of ~ 850 kV/cm. This outstanding energy density surpasses that of most previously reported lead-free
185 bulk ceramics. Concurrently, the energy storage efficiency (η , orange curve) demonstrates excellent
186 stability, maintaining a high value across the entire measurement range. Even at the maximum electric
187 field, the efficiency remains high at over 80%.

188 The simultaneous achievement of ultrahigh energy density and high efficiency is a significant break-
189 through. This exceptional performance is a direct manifestation of the desirable material characteris-
190 tics predicted and targeted by the AI Materials Scientist. The high breakdown strength is underpinned
191 by the dense, fine-grained microstructure discussed previously, while the high efficiency is a direct
192 result of the strong relaxor behavior induced by the high-entropy design, as evidenced by the slim
193 P-E loops. These results experimentally confirm the AI's success in identifying a novel compo-
194 sition within the vast chemical space that overcomes the typical trade-off between energy density
195 and efficiency, thereby validating this AI-driven approach as a powerful paradigm for discovering
196 next-generation materials.

197 3.4 Analysis of the AI agent's recommendation

198 The successful synthesis and verification of this high-performance ceramic serve as a pivotal validation
199 of our AI Materials Scientist's predictive capabilities. The central question remains: how did the agent
200 navigate the near-infinite chemical space to pinpoint this specific, non-intuitive composition? The
201 agent's success can be attributed to its ability to identify and optimize the highly complex, non-linear
202 relationships between composition, structure, and properties—a task that is exceptionally challenging

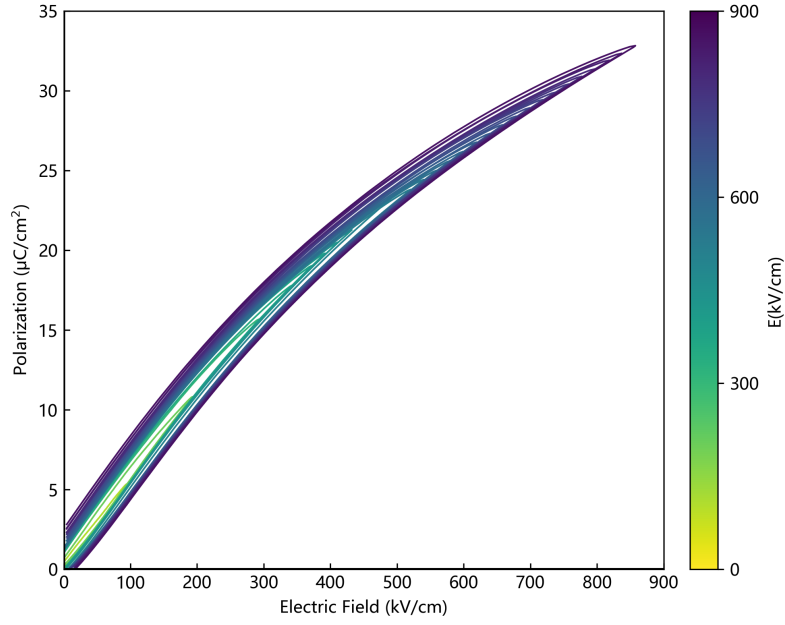


Figure 3: Unipolar polarization-electric field (P-E) hysteresis loops of the high-entropy ceramic measured at room temperature under various electric fields up to ~ 850 kV/cm. The color bar indicates the magnitude of the applied electric field.

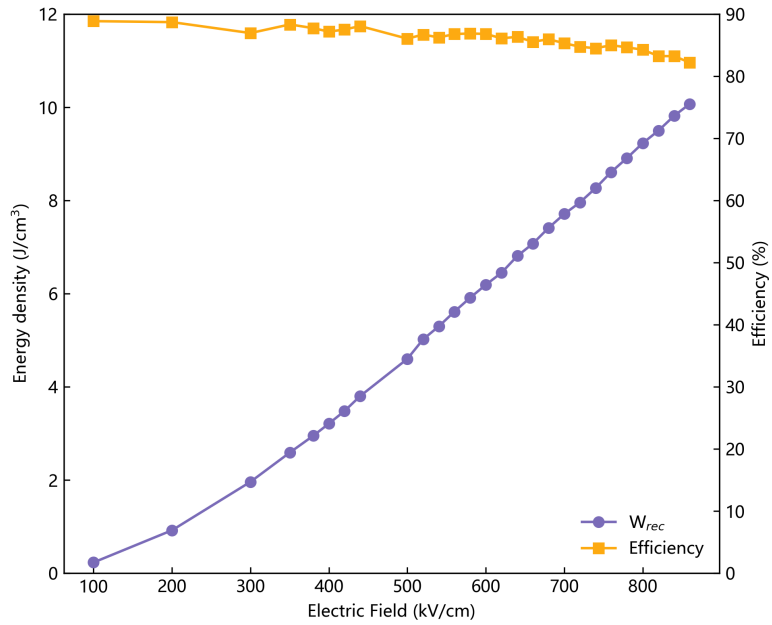


Figure 4: Recoverable energy storage density and energy storage efficiency as a function of the applied electric field for the high-entropy ceramic at room temperature.

203 for human researchers. By analyzing the chosen components, we can deconstruct the sophisticated
204 design strategy the agent likely discovered:

205 **A synergistic strategy for polarization and breakdown strength** The agent did not simply
206 maximize a single parameter but instead learned to strike a delicate balance. It selected components
207 with distinct, complementary functions:

- 208 • **High-polarization sources:** BaTiO₃ and BiFeO₃ are canonical ferroelectrics known to
209 provide a high maximum polarization (P_{\max}), a prerequisite for high energy density.
- 210 • **Relaxor and linearity inducers:** The agent simultaneously introduced components known
211 to disrupt long-range ferroelectric order. The inclusion of Bi_{0.5}Na_{0.5}TiO₃ (BNT) and the
212 overall high-entropy state—derived from mixing five distinct A-site cations—promotes the
213 formation of polar nanoregions (PNRs) instead of large ferroelectric domains. This is the
214 key to achieving the slim, relaxor-type P-E loops, which ensures low energy loss and high
215 efficiency.
- 216 • **Breakdown strength enhancers:** As a wide-bandgap linear dielectric, CaZrO₃ is known to
217 significantly increase the breakdown strength (E_b) and thermal stability of titanate-based
218 perovskites. The agent identified this crucial role and assigned it a substantial fraction (19%)
219 to elevate the breakdown strength to the experimentally observed high of \sim 850 kV/cm.

220 **Implicit optimization of microstructure** The composition recommended by the AI implicitly
221 promotes the ideal microstructure observed in the SEM analysis. The chemical complexity and the
222 presence of ions such as Zr⁴⁺ and La³⁺ can act as grain growth inhibitors during sintering. By
223 learning from thousands of literature examples, the agent likely correlated specific compositional
224 features with the formation of dense, fine-grained microstructures. It “understood” that achieving
225 superior intrinsic properties is futile without also ensuring the optimal extrinsic microstructure (i.e.,
226 high density and fine grains) required to realize those properties in a bulk ceramic. Therefore, the
227 agent effectively solved a multi-objective optimization problem, concurrently targeting electronic
228 properties and the microstructural features that enable them.

229 **4 Limitations and future directions**

230 Despite its remarkable success, the current AI Materials Scientist agent has several limitations that
231 represent important directions for future research:

232 **The “black box” problem** While we can rationalize the agent’s choice post-hoc, its internal
233 decision-making process remains largely opaque. The agent does not explicitly state why it chose
234 a particular ratio, making it difficult to extract new, fundamental scientific principles from its
235 recommendations. Future work will focus on implementing Explainable AI (XAI) techniques to
236 enhance the model’s transparency and interpretability.

237 **Data dependency** The agent’s knowledge is bounded by its training data. It excels at interpolating
238 and discovering novel combinations within known chemical systems but struggles to extrapolate and
239 propose materials containing entirely new elements or crystal structures not well-represented in the
240 literature. Expanding the training datasets and developing physics-informed neural networks are
241 crucial next steps.

242 **Neglect of synthesis feasibility** The current agent predicts a target composition but offers no
243 guidance on the experimental synthesis route (e.g., sintering temperature, duration, atmosphere).
244 The actual fabrication process still relies on human expertise. A key future objective is to develop
245 a system that co-predicts the composition, its properties, and the optimal processing parameters
246 required to create it.

247 **5 Conclusion**

248 In this study, we have successfully demonstrated the power of an AI-driven approach to accelerate
249 the discovery of high-performance materials. By deploying an ‘AI Materials Scientist’, we navigated

250 the vast and complex compositional space of high-entropy ceramics to design a novel lead-free
251 dielectric material, $0.36\text{BaTiO}_3 - 0.32\text{BiFeO}_3 - 0.09\text{Bi}_{0.5}\text{Na}_{0.5}\text{TiO}_3 - 0.19\text{CaZrO}_3 - 0.04\text{Sr}_{0.7}\text{La}_{0.2}\text{TiO}_3$.
252 Experimental validation confirmed the AI's design, revealing a single-phase perovskite structure
253 with a dense, fine-grained microstructure. This ceramic exhibits a remarkable combination of a
254 high recoverable energy density of 10 J/cm^3 and a superior efficiency of 80%, marking a significant
255 advancement for lead-free energy storage materials.

256 The success of this work highlights the ability of AI to overcome the limitations of conventional
257 Edisonian research, identifying a non-intuitive composition that synergistically optimizes multiple
258 competing properties. The AI agent effectively learned the complex interplay between composition,
259 crystal structure, microstructure, and performance, delivering a material that solves the long-standing
260 trade-off between energy density and efficiency. This research serves as a powerful testament to the
261 paradigm shift AI represents for materials science, transforming it from a process of intuition-based
262 iteration to one of data-driven, accelerated discovery. Future work will focus on enhancing the AI's
263 interpretability and expanding its predictive capabilities to include synthesis protocols, further closing
264 the loop on fully autonomous materials research and paving the way for the rapid development of
265 next-generation materials for a sustainable future.

266 **6 Reproducibility Statement**

267 **6.1 Reproducibility of Core Findings**

268 All materials synthesis, characterization, and performance testing reported in this manuscript adhere
269 to standard experimental procedures. We have provided comprehensive details of the experimental
270 parameters, equipment models, and chemical reagent specifications in the Methods section. We are
271 confident that the core materials and their corresponding performance data presented herein are fully
272 reproducible by following the detailed steps described.

273 **6.2 Note on AI-Generated Content**

274 The "AI Material Scientist" framework utilized in this study is powered by a large language model.
275 We hereby state that due to the inherent stochasticity of such models, repeated runs with the same
276 input prompts will not guarantee identical scientific hypotheses or experimental protocols in every
277 instance. This variability is a known characteristic of current generative AI technologies.

278 **6.3 Reproducibility of the Framework and Methodology**

279 Notwithstanding the non-deterministic nature of single-pass generation, the overall framework of
280 **AI-driven hypothesis generation and validation** proposed herein is robust and reproducible. We
281 believe that any researcher with relevant domain expertise can independently leverage our described
282 framework, model (if open-sourced) or a similar model, to develop research pathways for discovering
283 novel high-performance materials. The significance of this paper lies not only in the specific material
284 reported but also in demonstrating the profound potential of this AI framework to accelerate materials
285 discovery.

286 We firmly believe that the deep integration of artificial intelligence with materials science for generat-
287 ing hypotheses and designing experiments is a promising and reproducible direction for the future of
288 materials research and development. We encourage our peers in the scientific community to adopt
289 and extend the framework presented in this work to collectively advance the intelligent discovery of
290 high-performance materials.

291 **References**

- 292 [1] Peng, Z., Wang, C., Chen, X., & Chen, Z. (2021) Strategies to Improve the Energy Storage Properties of
293 Perovskite Lead-Free Relaxor Ferroelectrics: A Review. *Advanced Energy Materials* **11**(23):2100121.
294 [2] Li, F., Zhai, J., Shen, B., Liu, X., & Zhang, H. (2018) Recent progress of lead-free energy-storage ferroelectric
295 ceramics. *Journal of Advanced Ceramics* **7**(3):195–208.

- 296 [3] Yang, L., Kong, X., Li, F., Hao, H., Cheng, Z., Liu, H., Li, J.-F., & Zhang, S. (2019) Perovskite lead-free
297 dielectrics for energy storage applications. *Progress in Materials Science* **102**:72–108.
- 298 [4] Zhao, P., Wang, H., Wu, L., Chen, L., Cai, Z., Li, L., & Wang, X. (2019) High-performance relaxor
299 ferroelectric materials for energy storage applications. *Advanced Energy Materials* **9**(42):1803048.
- 300 [5] Li, J., Li, F., Xu, Z., & Zhang, S. (2018) Multilayer lead-free ceramic capacitors with ultrahigh energy density
301 and efficiency. *Advanced Materials* **30**(32):1802155.
- 302 [6] Pan, H., Li, F., Liu, Y., Zhang, Q., Wang, M., Lan, S., Zheng, Y., Ma, J., Gu, L., Shen, Y., Yu, P., Zhang, S.,
303 Chen, L.-Q., Lin, Y.-H., & Nan, C.-W. (2018) Ultrahigh-energy density lead-free dielectric films via polymorphic
304 nanodomain design. *Science* **365**:578–582.
- 305 [7] Yao, Z., Song, Z., Hao, H., Yu, Z., Cao, M., Zhang, S., Lanagan, M. T., & Liu, H. (2017)
306 Homogeneous/Inhomogeneous-Structured Dielectrics and their Energy-Storage Performances. *Advanced Mate-
307 rials* **29**(20):1601727.
- 308 [8] Wang, D., Fan, Z., Li, W., Zhou, D., Feteira, A., Wang, G., Murakami, S., Sun, S., Zhao, Q., Tan, X., &
309 Reaney, I. M. (2021) High energy storage density and large strain in $\text{Bi}(\text{Zn}_{2/3}\text{Nb}_{1/3})\text{O}_3$ -doped BiFeO_3 – BaTiO_3
310 ceramics. *ACS Applied Energy Materials* **3**(2):1034–1042.
- 311 [9] Chen, H., Shi, J., Chen, X., Zhou, M., He, X., Wang, F., Luo, L., Li, Y., & Zhou, C. (2020) High entropy
312 $(\text{Bi}_{0.2}\text{Na}_{0.2}\text{K}_{0.2}\text{Ba}_{0.2}\text{Ca}_{0.2})\text{TiO}_3$ ceramic with superior energy storage performance. *Journal of Materials
313 Chemistry A* **8**(31):15958–15968.
- 314 [10] Ye, Y., Ren, S., Gao, B., Zhou, X., Yang, S., Hao, X., & Wu, H. (2021) High-entropy design for superior
315 capacitive energy storage performance in lead-free ceramics. *Journal of Materials Chemistry A* **9**(35):19697–
316 19706.
- 317 [11] Oses, C., Toher, C., & Curtarolo, S. (2020) High-entropy ceramics. *Nature Reviews Materials* **5**(4):295–309.
- 318 [12] Balachandran, P. V., Kowalski, B., Sehirlioglu, A., & Lookman, T. (2018) Experimental search for high-
319 temperature ferroelectric perovskites guided by two-step machine learning. *Nature Communications* **9**(1):1668.
- 320 [13] Lookman, T., Balachandran, P. V., Xue, D., & Yuan, R. (2019) Active learning in materials science with
321 emphasis on adaptive sampling using uncertainties for targeted design. *npj Computational Materials* **5**(1):21.
- 322 [14] Schmidt, J., Marques, M. R. G., Botti, S., & Marques, M. A. L. (2019) Recent advances and applications of
323 machine learning in solid-state materials science. *npj Computational Materials* **5**(1):83.
- 324 [15] Butler, K. T., Davies, D. W., Cartwright, H., Isayev, O., & Walsh, A. (2018) Machine learning for molecular
325 and materials science. *Nature* **559**(7715):547–555.
- 326 [16] Wang, G., Lu, Z., Li, Y., Li, L., Ji, H., Feteira, A., Zhou, D., Wang, D., Zhang, S., & Reaney, I. M. (2021)
327 Electroceramics for high-energy density capacitors: Current status and future perspectives. *Chemical Reviews*
328 **121**(10):6124–6172.
- 329 [17] Zhao, L., Liu, Q., Gao, J., Zhang, S., & Li, J. F. (2017) Lead-free antiferroelectric silver niobate tantalate
330 with high energy storage performance. *Advanced Materials* **29**(31):1701824.
- 331 [18] Sanchez-Lengeling, B., & Aspuru-Guzik, A. (2018) Inverse molecular design using machine learning:
332 Generative models for matter engineering. *Science* **361**(6400):360–365.

333 **Agents4Science AI Involvement Checklist**

- 334 1. **Hypothesis development:** Hypothesis development includes the process by which you
335 came to explore this research topic and research question. This can involve the background
336 research performed by either researchers or by AI. This can also involve whether the idea
337 was proposed by researchers or by AI.

338 Answer: **[C]**

339 Explanation: Human researchers identified the research direction of high-performance
340 energy storage ceramics, and the AI Materials Scientist proposed the design of high-entropy
341 ceramics.

- 342 2. **Experimental design and implementation:** This category includes design of experiments
343 that are used to test the hypotheses, coding and implementation of computational methods,
344 and the execution of these experiments.

345 Answer: **[D]**

346 Explanation: The AI Materials Scientist designed the experiment and drove the autonomous
347 experimental platform to conduct it, with human assistance under the AI's direction for
348 certain steps that the platform cannot yet complete, such as polishing the ceramic pellets.

- 349 3. **Analysis of data and interpretation of results:** This category encompasses any process to
350 organize and process data for the experiments in the paper. It also includes interpretations of
351 the results of the study.

352 Answer: **[D]**

353 Explanation: The analysis of experimental data (such as XRD, SEM, P-E loops) and the
354 scientific interpretations presented in the paper were all completed by the AI Materials
355 Scientist.

- 356 4. **Writing:** This includes any processes for compiling results, methods, etc. into the final
357 paper form. This can involve not only writing of the main text but also figure-making,
358 improving layout of the manuscript, and formulation of narrative.

359 Answer: **[D]**

360 Explanation: The main writing of the paper, including the creation of all figures, was
361 completed by the AI. The role of humans was not that of a primary author, but rather to
362 guide the AI's writing direction through a few prompts. All textual content was generated
363 by the AI.

- 364 5. **Observed AI Limitations:** What limitations have you found when using AI as a partner or
365 lead author?

366 Description: Agents perform well on well-designed, structured tasks. However, they face
367 significant difficulties with tasks that are overly open-ended or have not been specifically
368 engineered for them. For instance, in our work, we have meticulously designed an intelligent
369 agent for materials research and development. This agent is highly effective at its designated
370 task of discovering high-performance materials, but its performance in academic paper
371 writing is considerably weaker.

372 **Agents4Science Paper Checklist**

373 **1. Claims**

374 Question: Do the main claims made in the abstract and introduction accurately reflect the
375 paper's contributions and scope?

376 Answer: [Yes]

377 Justification: The abstract and introduction of this paper clearly articulate the core arguments
378 and precisely define the scope of the research. These arguments are thoroughly and
379 convincingly supported in the experimental results and analysis section.

380 Guidelines:

- 381 • The answer NA means that the abstract and introduction do not include the claims
382 made in the paper.
- 383 • The abstract and/or introduction should clearly state the claims made, including the
384 contributions made in the paper and important assumptions and limitations. A No or
385 NA answer to this question will not be perceived well by the reviewers.
- 386 • The claims made should match theoretical and experimental results, and reflect how
387 much the results can be expected to generalize to other settings.
- 388 • It is fine to include aspirational goals as motivation as long as it is clear that these goals
389 are not attained by the paper.

390 **2. Limitations**

391 Question: Does the paper discuss the limitations of the work performed by the authors?

392 Answer: [Yes]

393 Justification: In the paper, there is a section discussing the limitations.

394 Guidelines:

- 395 • The answer NA means that the paper has no limitation while the answer No means that
396 the paper has limitations, but those are not discussed in the paper.
- 397 • The authors are encouraged to create a separate "Limitations" section in their paper.
- 398 • The paper should point out any strong assumptions and how robust the results are to
399 violations of these assumptions (e.g., independence assumptions, noiseless settings,
400 model well-specification, asymptotic approximations only holding locally). The authors
401 should reflect on how these assumptions might be violated in practice and what the
402 implications would be.
- 403 • The authors should reflect on the scope of the claims made, e.g., if the approach was
404 only tested on a few datasets or with a few runs. In general, empirical results often
405 depend on implicit assumptions, which should be articulated.
- 406 • The authors should reflect on the factors that influence the performance of the approach.
407 For example, a facial recognition algorithm may perform poorly when image resolution
408 is low or images are taken in low lighting.
- 409 • The authors should discuss the computational efficiency of the proposed algorithms
410 and how they scale with dataset size.
- 411 • If applicable, the authors should discuss possible limitations of their approach to
412 address problems of privacy and fairness.
- 413 • While the authors might fear that complete honesty about limitations might be used by
414 reviewers as grounds for rejection, a worse outcome might be that reviewers discover
415 limitations that aren't acknowledged in the paper. Reviewers will be specifically
416 instructed to not penalize honesty concerning limitations.

417 **3. Theory assumptions and proofs**

418 Question: For each theoretical result, does the paper provide the full set of assumptions and
419 a complete (and correct) proof?

420 Answer: [NA]

421 Justification: The paper does not include theoretical results.

422 Guidelines:

- 423 • The answer NA means that the paper does not include theoretical results.
424 • All the theorems, formulas, and proofs in the paper should be numbered and cross-
425 referenced.
426 • All assumptions should be clearly stated or referenced in the statement of any theorems.
427 • The proofs can either appear in the main paper or the supplemental material, but if
428 they appear in the supplemental material, the authors are encouraged to provide a short
429 proof sketch to provide intuition.

430 **4. Experimental result reproducibility**

431 Question: Does the paper fully disclose all the information needed to reproduce the main ex-
432 perimental results of the paper to the extent that it affects the main claims and/or conclusions
433 of the paper (regardless of whether the code and data are provided or not)?

434 Answer: [Yes]

435 Justification: The paper includes the test results of the prepared ceramic materials, and the
436 experimental steps are described such that the preparation of the ceramic materials can be
437 reproduced.

438 Guidelines:

- 439 • The answer NA means that the paper does not include experiments.
440 • If the paper includes experiments, a No answer to this question will not be perceived
441 well by the reviewers: Making the paper reproducible is important.
442 • If the contribution is a dataset and/or model, the authors should describe the steps taken
443 to make their results reproducible or verifiable.
444 • We recognize that reproducibility may be tricky in some cases, in which case authors
445 are welcome to describe the particular way they provide for reproducibility. In the case
446 of closed-source models, it may be that access to the model is limited in some way
447 (e.g., to registered users), but it should be possible for other researchers to have some
448 path to reproducing or verifying the results.

449 **5. Open access to data and code**

450 Question: Does the paper provide open access to the data and code, with sufficient instruc-
451 tions to faithfully reproduce the main experimental results, as described in supplemental
452 material?

453 Answer: [No]

454 Justification: Due to the highly domain-specific nature of our framework, it cannot be
455 directly utilized or validated by researchers outside the ceramic materials field. Furthermore,
456 as related research is still ongoing, we have chosen not to open-source the code at this time.
457 The code will be made publicly available once our follow-up studies are completed. The
458 experimental data supporting the conclusions of this paper can be independently reproduced
459 by following the ceramic material synthesis steps as described in the Methods section.

460 Guidelines:

- 461 • The answer NA means that paper does not include experiments requiring code.
462 • Please see the Agents4Science code and data submission guidelines on the conference
463 website for more details.
464 • While we encourage the release of code and data, we understand that this might not be
465 possible, so “No” is an acceptable answer. Papers cannot be rejected simply for not
466 including code, unless this is central to the contribution (e.g., for a new open-source
467 benchmark).
468 • The instructions should contain the exact command and environment needed to run to
469 reproduce the results.
470 • At submission time, to preserve anonymity, the authors should release anonymized
471 versions (if applicable).

472 **6. Experimental setting/details**

473 Question: Does the paper specify all the training and test details (e.g., data splits, hyper-
474 parameters, how they were chosen, type of optimizer, etc.) necessary to understand the
475 results?

476 Answer: [Yes]

477 Justification: The experimental data can be independently reproduced by following the
478 ceramic material synthesis steps as described in the Methods section.

479 Guidelines:

- 480 • The answer NA means that the paper does not include experiments.
481 • The experimental setting should be presented in the core of the paper to a level of detail
482 that is necessary to appreciate the results and make sense of them.
483 • The full details can be provided either with the code, in appendix, or as supplemental
484 material.

485 **7. Experiment statistical significance**

486 Question: Does the paper report error bars suitably and correctly defined or other appropriate
487 information about the statistical significance of the experiments?

488 Answer: [No]

489 Justification: As the wet-lab experiment was performed in a single iteration, error bars are
490 not reported.

491 Guidelines:

- 492 • The answer NA means that the paper does not include experiments.
493 • The authors should answer "Yes" if the results are accompanied by error bars, confi-
494 dence intervals, or statistical significance tests, at least for the experiments that support
495 the main claims of the paper.
496 • The factors of variability that the error bars are capturing should be clearly stated
497 (for example, train/test split, initialization, or overall run with given experimental
498 conditions).

499 **8. Experiments compute resources**

500 Question: For each experiment, does the paper provide sufficient information on the com-
501 puter resources (type of compute workers, memory, time of execution) needed to reproduce
502 the experiments?

503 Answer: [NA]

504 Justification: Our work involves wet-lab experiments, not computer experiments.

505 Guidelines:

- 506 • The answer NA means that the paper does not include experiments.
507 • The paper should indicate the type of compute workers CPU or GPU, internal cluster,
508 or cloud provider, including relevant memory and storage.
509 • The paper should provide the amount of compute required for each of the individual
510 experimental runs as well as estimate the total compute.

511 **9. Code of ethics**

512 Question: Does the research conducted in the paper conform, in every respect, with the
513 Agents4Science Code of Ethics (see conference website)?

514 Answer: [Yes]

515 Justification: The research conducted in the paper conforms with the Agents4Science Code
516 of Ethics.

517 Guidelines:

- 518 • The answer NA means that the authors have not reviewed the Agents4Science Code of
519 Ethics.
520 • If the authors answer No, they should explain the special circumstances that require a
521 deviation from the Code of Ethics.

522 **10. Broader impacts**

523 Question: Does the paper discuss both potential positive societal impacts and negative
524 societal impacts of the work performed?

525 Answer: [NA]

526 Justification: This paper focuses specifically on agents for materials science, as such,
527 considerations of broader societal impact fall beyond its defined scope.

528 Guidelines:

- 529 • The answer NA means that there is no societal impact of the work performed.
530 • If the authors answer NA or No, they should explain why their work has no societal
531 impact or why the paper does not address societal impact.
532 • Examples of negative societal impacts include potential malicious or unintended uses
533 (e.g., disinformation, generating fake profiles, surveillance), fairness considerations,
534 privacy considerations, and security considerations.
535 • If there are negative societal impacts, the authors could also discuss possible mitigation
536 strategies.